East European Journal of Physics. **3**. 378-384 (2026)
DOI:10.26565/2312-4334-2026-3-33 ISSN 2312-4334

EFFECT OF ELECTROLYTE CONCENTRATION AND DISCHARGE FREQUENCY ON Ti-6Al-4V POWDER PARTICLE SIZE DISTRIBUTION OBTAINED BY ECDM

B.A. G'oipov*, A.A. Zaripov, U.F. Berdiyev, Sh.Ch. Iskandarov, T.K. Turdaliev, S.A. Tulaganov
Institute of Ion-Plasma and Laser Technologies named after U.A. Arifov, Academy of Sciences of the Republic of Uzbekistan, 100125, Durmon yuli st 33, Tashkent, Uzbekistan
**Corresponding Author email: goipovbunyod7@gmail.com*
Received April 27, 2026; revised July 31, 2026; accepted August 3, 2026

This study investigates the distribution of Ti-6Al-4V alloy powder microparticles used in 3D printing under different discharge frequencies and NaCl electrolyte concentrations. This work analyzed the process for obtaining monodisperse Ti-6Al-4V alloy powders using the Electrochemical Discharge Machining (ECDM) method. The results showed that an optimal NaCl electrolyte concentration of 30 g/L ensures stable plasma channel formation and a narrow particle size distribution. Regression analysis and low standard error values (0.00386–0.00834) confirm the process's high controllability. The effect of frequency on particle size was also investigated: at 3.2 kHz, the minimum average particle size of 16.598 μm was recorded, whereas increasing the frequency to 32 kHz increased particle size to 28.063 μm due to thermal accumulation. The results indicate that at both 3.2 kHz and 32 kHz frequencies, 58.24% to 68.89% of the produced powders fall within the 15–55 μm range required for PBF-LB/M technology. These findings demonstrate the suitability of the obtained powders for additive manufacturing technologies.
Keywords: *Ti-6Al-4V powder; ECDM; Additive manufacturing; NaCl electrolyte; Electrolyte concentration; Particle size distribution; Frequency; Regression analysis*

INTRODUCTION

The increasing prevalence of orthopedic and dental diseases worldwide has driven steady growth in demand for implants made from biomedical titanium (Ti) and its alloys [1]. Fabricating these implants using additive manufacturing (AM) technologies allows production of 3D shapes with high geometric accuracy while ensuring maximum conformity to individual anatomical structures [2]. Such biocompatible implants are primarily made from the Ti-6Al-4V alloy. Owing to its low thermal conductivity and density, high strength, favorable strength-to-weight ratio, and excellent resistance to temperature and corrosion, Ti-6Al-4V finds wide application in aerospace and defense [3], automotive [4], shipbuilding [5], energy [6], petrochemical industries [7], as well as in medical instruments and implants [8].

In these fields, Ti-6Al-4V alloy powders are used in AM processes, specifically PBF-LB/M (Powder Bed Fusion – Laser Beam/Metal) 3D printing. In these processes, particle shape, chemical purity, and particle size distribution are critical [9], as larger particle sizes reduce the surface area available for laser energy absorption [10], necessitating higher laser energy input [11]. Fine powders allow higher packing density but may increase internal defects in the fabricated part [12].

Metal powders are produced with various size distributions using mechanical [13], chemical [14], and physical [15] methods, often resulting in irregular shapes, rough surface textures, internal porosity, and uneven surface morphology. Furthermore, these production methods require complex equipment and high costs, which can lead to variability in powder flowability [16], density, melting behavior, part surface quality, porosity [17], and mechanical properties [18], as well as increase production costs [19, 20].

The particle size distribution of powders produced by the above methods ranges from 0–250 μm, and in PBF-LB/M powder spreading technologies, particles larger than 45 μm [21] require additional processing [22]. Reprocessing Ti-6Al-4V powders, however, significantly increases oxygen content [23]. To address these limitations, recent studies have increasingly focused on unconventional methods for producing metal powders, particularly via electrical discharge machining (EDM) [24]. This approach enables the production of nano [25] and micro-sized particles of metals [26] and their alloys [27] in dielectric media [28].

An additional advantage of this method is that particle size distribution can be controlled by adjusting the current, frequency [29], discharge energy, and machining depth [30]. To further optimize these parameters, various alloys, metal powders, and salts are added to the dielectric fluid to improve its electrical conductivity, allowing the use of electrolytes instead of conventional dielectric fluids. This method, known as Electrochemical Discharge Machining (ECDM), operates at lower current levels compared to EDM and can reduce energy consumption and costs while preserving particle size distribution [31].

In ECDM, the surrounding medium plays a crucial role, as the machining rate is often closely related to the properties of the medium [32-34]. Although considerable work has been conducted on process efficiency, data on the effect of the

Cite as: B.A. G'oipov, A.A. Zaripov, U.F. Berdiyev, Sh.Ch. Iskandarov, T.K. Turdaliev, S.A. Tulaganov, East Eur. J. Phys. 3, 378 (2026), https://doi.org/10.26565/2312-4334-2026-3-33

medium on particle size distribution remain insufficient [35]. Previous studies have employed fluids that affect the final product quality [36], overly aggressive media [37], or fluids that require high-energy input and increase brittleness in the final product [38]. Based on the above, selecting a fluid medium for ECDM that ensures particle size distribution without affecting the quality of the final product remains a highly pressing challenge [31–38]. This scientific article is devoted to practical solutions to this critical issue.

In this study, the production of Ti-6Al-4V powders using various electrolytes in the ECDM process and the investigation of their particle size distribution are proposed.

EXPERIMENTAL PROCEDURE

The synthesis of Ti-6Al-4V alloy-based powder was carried out on an experimental setup designed for ECDM, the schematic diagram of which is shown in Figure 1. The key feature of the system is a pulsed power supply assembled using high-speed IRG4P50UD IGBT switches and 150EBU04 diodes. This control architecture enables precise adjustment of the process parameters, including voltage amplitude up to 400 V, current up to 20 A, and pulse modulation frequency up to 100 kHz.

To generate a stable spark discharge, the anode was fully immersed in the electrolyte, while the vertically aligned cylindrical cathode, positioned above it, was submerged to a depth of 1–5 mm. The stability of the physicochemical conditions in the reaction zone was maintained by a filtration system and forced circulation of the working fluid. A pump with a flow rate of 2 L/min was used to ensure liquid circulation. This provided efficient heat removal and rapid evacuation of erosion products from the interelectrode gap, preventing thermal degradation of the microstructures, re-melting, and uncontrolled coagulation (agglomeration).

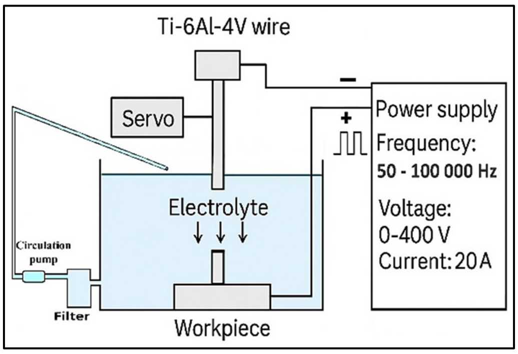

Figure 1. Schematic diagram of the ECDM setup.

For powder production, electrodes with a diameter of 4 mm made of biocompatible Ti-6Al-4V alloy were used. The electrodes were immersed in an aqueous NaCl electrolyte with concentrations of 10–60 g/L, where a negative potential was applied to the cathode and a positive potential to the anode.

As shown in the schematic, the electrodes were submerged in a vessel filled with the working electrolyte (vessel volume: 2 L). A servo system controlled the interelectrode gap and ensured the stability of micro-discharges. Rod electrodes with a diameter of 4 mm fabricated from biocompatible Ti-6Al-4V alloy were employed. During the experiments, a DC voltage of up to 280 V was applied to the system, while the control unit provided pulse generation with frequencies up to 32 kHz. The current was maintained at up to 0.6 A, which allowed stable spark discharge conditions to be sustained.

To prepare the working medium (electrolyte), deionized water with a specific resistivity of 18 MΩ·cm was used. NaCl of chemically pure (“CP”) grade was added to the water at concentrations of 10, 30, and 60 g/L. The amount of reagents was controlled using an analytical balance with an accuracy of ±0.001 g. The applied high-frequency pulsed operating mode enabled direct localization of energy within the spark discharge channel. This minimized undesirable electrolysis effects and ensured the dominant contribution of electro-spark processes in the electrolyte to the formation of the phase composition of microparticles.

The particles formed after discharge were separated from the working solution using a Hittech “EBA 20S” centrifuge at a rotation frequency of 60 s^{-1} for 5 minutes. The obtained precipitate was dried in a FAITHFUL SH-6C drying oven at 70 °C for 24 hours. Particle size distribution was determined using a WJL-602 laser particle size analyzer. This instrument, operating with a He–Ne laser (λ = 632.8 nm), provides measurements in the range of 0.1–800 μm with an accuracy of ±0.5%. The analysis was performed in distilled water at a particle concentration of 1.5–1.7%.

The obtained experimental data were processed and analyzed using OriginPro 9.1 software. The measurement error of the data did not exceed 3%.

RESULTS AND DISCUSSION

Initially, the granulometric analysis of Ti-6Al-4V alloy powder obtained by the ECDM method was performed using a laser particle analyzer (Table 1). The table presents the analysis results of powder particles obtained under identical voltage and current conditions, but at three different NaCl electrolyte concentrations.

Table 1. Granulometric analysis of powder obtained at different concentrations using a laser particle analyzer.

NaCl concentration in deionized water	D_3, µm	D_{10}, µm	D_{50}, µm	D_{av}, µm	D_{90}, µm	D_{97}, µm
10 g/L NaCl	4.585	7.659	25.631	29.082	58.684	78.369
30 g/L NaCl	3.212	4.777	12.909	16.598	30.223	40.372
60 g/L NaCl	4.074	6.405	20.254	23.968	46.727	61.246

For example, the value of 4.585 µm in the D3 column for a 10 g/L NaCl solution indicates that 3% of the particles are smaller than this size. Similarly, the D10, D50, D90, and D97 parameters represent that 10%, 50%, 90%, and 97% of the particles, respectively, are smaller than the given size. Dav denotes the average particle size of the powder.

Based on experiments conducted at different NaCl concentrations and a frequency of 0.32 kHz, the obtained powder samples were analyzed using a laser particle analyzer (Figure 2).

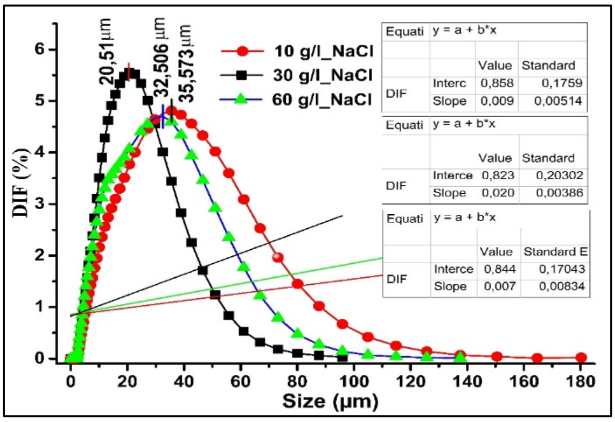

Figure 2. Dependence of particle size distribution on concentration

The graph presents the linear particle size distribution of powders obtained at three different NaCl concentrations (10 g/L, 30 g/L, and 60 g/L), where the X-axis represents particle size and the Y-axis shows the quantitative fraction of particles (differential distribution, DIF %). As can be seen from the graph, the distribution of particles obtained at a 30 g/L concentration is relatively narrow. To quantify the narrowness of the distribution, the initial growth dynamics of the differential distribution (DIF %) were analyzed using a linear regression function (y = a + bx). From a mathematical and statistical perspective, the slope coefficient (Slope) in the graph reflects the intensity of particle formation and growth dynamics. The intercept represents the initial parameter of the linear relationship and is nearly identical for all cases. The standard error indicates the average deviation between experimental measurements.

The results of the linear regression analysis show that at the minimum electrolyte concentration of 10 g/L, the slope coefficient is 0.009, which is a low value. This low value indicates a reduced number of ions, low current density, and low ion mobility, resulting in an unstable plasma channel with localized energy accumulation. This energetic state leads to a significant broadening of the particle size distribution, i.e., polydispersity. This is also confirmed by the large difference between the peak of the differential distribution (DIF = 35.573 µm) and the average particle size (Dav = 29.082 µm, see Table 1).

At the highest electrolyte concentration of 60 g/L, the lowest slope coefficient (0.007) and the highest standard error (0.00834) were recorded. In this case, due to the high concentration, the number of ions increases, current density and ion mobility become higher, and a longer plasma lifetime leads to the formation of larger particles. The average particle size was 23.968 µm, while the maximum DIF peak reached 32.506 µm, indicating a wide particle size distribution.

The graph shows that at 30 g/L concentration, the slope value of 0.02 corresponds to the highest particle growth dynamics, while the standard error of 0.00386 is the lowest. This indicates the most balanced relationship between particle size and their quantitative fraction. The peak of the DIF distribution at 20.51 µm and the average particle size of 16.598 µm (see Table 1) confirm a narrow size distribution.

At this concentration, the ion concentration is sufficient, the electrolyte conductivity and ion mobility are high. The plasma lifetime is short and periodically reproducible. The energy exchange between the plasma channel and electrolyte is optimal, and the balance between discharge energy ensures the preservation of a narrow particle size distribution.

According to the results of the linear regression analysis, electrolyte concentration has a significant effect on particle formation and size distribution. At 10 g/L, low ion activity leads to increased polydispersity, while at 60 g/L, the formation of larger and non-uniform particles is observed. The most balanced condition is achieved at 30 g/L NaCl solution, where the slope and standard error reach optimal values. Under these conditions, a narrow particle size distribution is formed, indicating a monodisperse system. Therefore, 30 g/L NaCl solution is considered the optimal medium for producing stable and uniform Ti-6Al-4V powder particles in the ECDM process.

Based on this, the experimental conditions were optimized, and the granulometric analysis of Ti-6Al-4V alloy powder obtained by the ECDM method at different frequencies was performed using a laser particle analyzer (Table 2).

Table 2. Granulometric analysis of powder obtained at different frequencies using a laser particle analyzer.

№	*f*, kHz	D_{10}, µm	D_{50}, µm	D_{av} µm	D_{90}, µm	S/V, m²/cm³
1.	32	8.883	24.915	28.063	51.497	0.257
2.	3,2	4.777	12.909	16.598	30.223	0.463
3.	0.32	5.971	16.457	18.853	34.989	0.382
4.	0.032	6.154	18.34	21.28	40.232	0.338

The table presents the granulometric analysis results of powder particles obtained at different frequencies under identical voltage and current conditions and a 30 g/L NaCl electrolyte concentration. For example, at 32 kHz, D_{10} = 8.883 µm indicates that 10% of the particles are smaller than this size. Similarly, the D_{50} and D_{90} parameters represent that 50% and 90% of the particles, respectively, are smaller than the given size. The D_{50} value corresponds to the median particle size. Dav represents the average particle size of the powder particles. At the given frequency, the specific surface area to volume ratio is S/V = 0.257 m²/cm³.

As shown in the table, when the frequency increases from 0.032 kHz to 0.32 kHz, the average particle size (Dav) decreases from 21.28 µm to 18.853 µm. At these low frequencies, the number of impulses is low, but each impulse has high energy; in this regime, the plasma channel becomes more stable and the number of impulses increases. With the increase in impulse frequency, the particle size slightly decreases, and the specific surface area to volume ratio increases from 0.338 to 0.382 (see Table 2). This reduction in average particle size is explained by the increase in frequency.

At medium frequencies of 0.32 kHz and 3.2 kHz, the number of impulses is sufficient, and the plasma channel as well as plasma lifetime remain stable. As a result, the average particle size (Dav) decreases from 18.853 µm to 16.598 µm. The decrease in Dav at medium frequencies leads to an increase in S/V from 0.382 to 0.463. This indicates that the reduction in particle size stabilizes, and the role of discharge frequency in particle formation becomes more significant.

At the high frequency of 32 kHz, the increase in the number of impulses leads to stabilization of the plasma channel and localized heat accumulation. As a result, material re-melting and particle aggregation intensify. This causes an increase in the average particle size (Dav) from 16.598 µm to 28.063 µm. Due to particle coarsening, the S/V value decreases from 0.463 to 0.257.

Since Ti-6Al-4V alloy has low thermal conductivity, an increase in discharge frequency initially leads to particle fragmentation, increasing the surface-to-volume ratio (S/V). However, at very high frequencies, localized heat accumulation and re-melting processes intensify, resulting in particle aggregation and a decrease in the S/V value.

The above granulometric analysis results are summarized in a single graph (Figure 3), which illustrates the effect of discharge frequency on particle size and its distribution for powders obtained by the ECDM method.

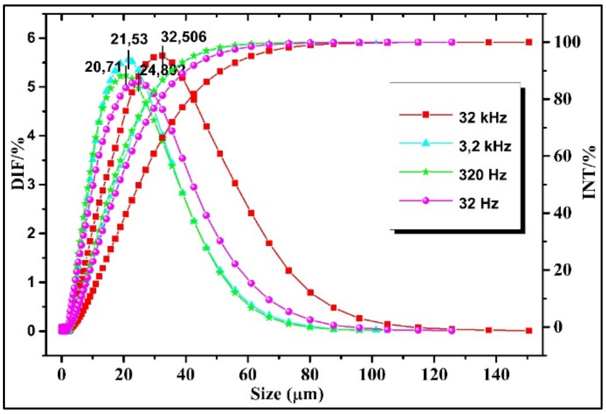

Figure 3. Particle size distribution of powders obtained in 30 g/L NaCl solution at different frequencies

The figure shows the differential (DIF %) and integral (INT %) particle size distributions of powders obtained at a frequency of 32 kHz, where the red curve represents the distribution. The X-axis represents the particle size in the range of 0.1–150.6 µm, while the left Y-axis shows the percentage fraction of particles corresponding to the differential distribution (DIF %). The right Y-axis represents the cumulative particle fraction in the integral distribution (INT %). The particle size distribution increases up to 0.1–32.506 µm, where the DIF peak reaches 5.64%, and in this range the INT distribution reaches 66.45%. After this point, the DIF curve decreases, and the INT value reaches 100% at 150.5 µm. At high frequencies, an increase in particle dispersion is observed, indicating a polydisperse distribution. However, the most suitable fraction for additive manufacturing is concentrated in the 15–45 µm (62.23%) and 15–55 µm (68.89%) ranges, which is higher compared to other samples.

For powders obtained at 3.2 kHz, the blue curve represents the differential (DIF %) and integral (INT %) distributions. The X-axis shows particle sizes in the range of 0.1–101.28 µm, while the left Y-axis indicates the percentage fraction of the most frequently occurring particle sizes. The right Y-axis shows the cumulative integral distribution (INT %). The particle size distribution increases up to 0.1–21.53 µm, where the DIF peak reaches 5.56%, and the INT value reaches 62.04%. After this point, the DIF curve decreases, and the INT distribution reaches 100% at 101.28 µm. The most suitable fraction for 3D printing is concentrated in the 15–45 µm (56.16%) and 15–55 µm (58.24%) ranges.

The analysis of powders obtained at 3.2 kHz and 32 kHz shows that in both cases the DIF and INT distributions confirm the presence of a polydisperse system. At the higher frequency (32 kHz), the particle size distribution is broader, indicating a higher degree of dispersion. At the lower frequency (3.2 kHz), the distribution is narrower and more uniform. In both cases, the most favorable fraction for additive manufacturing is within the 15–55 µm range, confirming its suitability for AM processes.

For powders obtained at 0.32 kHz, the light green curve represents the differential (DIF %) and integral (INT %) distributions. The X-axis covers particle sizes from 0.1–104.96 µm. The left Y-axis shows the percentage of the most frequently occurring particle sizes, while the right Y-axis represents the cumulative INT distribution. The particle size distribution increases up to 0.1–20.71 µm, where the DIF peak reaches 5.24%, and the INT distribution reaches 63.74%. After this point, the DIF curve decreases, and the INT distribution reaches 100% at 104.96 µm. The most suitable fraction for 3D printing is 15–45 µm (53.74%) and 15–55 µm (55.73%).

For powders obtained at 0.032 kHz, the pink curve represents the DIF (%) and INT (%) distributions. The X-axis covers particle sizes from 0.1–125.7 µm. The particle size distribution increases up to 0.1–24.802 µm, where the DIF peak reaches 5.1%, and the INT distribution reaches 66.88%. After this, the DIF curve decreases, and the INT distribution reaches 100% at 125.7 µm. The most suitable fractions for 3D printing are 15–45 µm (56.33%) and 15–55 µm (59.56%).

The granulometric analysis of powders obtained at 0.32 kHz and 0.032 kHz shows that the particle size is widely distributed. As the frequency decreases, the maximum particle size increases, and the distribution range broadens. At the same time, the fraction suitable for 3D printing (15–45 µm and 15–55 µm) remains dominant in both cases, with slightly higher values observed at 0.032 Hz.

The graph shows that discharge frequency significantly affects particle size and its distribution. As the frequency increases from 0.032 kHz to 3.2 kHz, the particle size decreases and the distribution becomes narrower. However, at 32 kHz, due to localized heat accumulation and particle aggregation, the particle size increases again and the distribution becomes broader. The most uniform and finest dispersed powder is obtained at 3.2 kHz.

CONCLUSIONS

The conducted study confirms that electrolyte concentration and discharge frequency strongly influence the granulometric composition and morphology of Ti-6Al-4V alloy powders in the ECDM process. According to linear regression analysis, a 30 g/L NaCl solution is the optimal concentration, where balanced Slope and Standard Error values lead to the formation of a monodisperse particle distribution.

As discharge frequency increases, particles initially undergo fragmentation, increasing the surface-to-volume ratio; however, at very high frequencies, localized heat accumulation and re-melting processes cause particle aggregation, resulting in a broader distribution. A frequency of 3.2 kHz provides a relatively narrow and uniform distribution, whereas at 32 kHz polydispersity increases.

Thus, a 30 g/L NaCl electrolyte solution combined with medium and high-frequency regimes was identified as optimal. Under these conditions, 58.24–68.89% of Ti-6Al-4V powder particles fall within the 15–55 µm range, which is suitable for 3D printing requirements.

Conflict of interest

The authors declare that they have no conflict of interest.

ORCID

B.A. G'oipov, https://orcid.org/0009-0005-3550-7893; **A.A. Zaripov,** https://orcid.org/0000-0003-4964-1776;
U.F. Berdiyev, https://orcid.org/0000-0003-2808-0105; **Sh.Ch. Iskandarov,** https://orcid.org/0000-0002-3002-9141;
T.K. Turdaliev, https://orcid.org/0000-0002-0732-9357; **S.A. Tulaganov,** https://orcid.org/0000-0003-1881-2165

REFERENCES

[1] Kacsó, A. B., & Peter, I. "A Review of Past Research and Some Future Perspectives Regarding Titanium Alloys in Biomedical Applications," Journal of Functional Biomaterials, **16**(4), 144 (2025). https://doi.org/10.3390/jfb16040144

[2] del Bosque, A., Fernández-Arias, P., & Vergara, D. "Titanium Additive Manufacturing with Powder Bed Fusion: A Bibliometric Perspective," Applied Sciences, **14**(22), 10543 (2024). https://doi.org/10.3390/app142210543

[3] Radhika, C., Shanmugam, R., Ramoni, M., & Gnanavel, B. K. "A review on additive manufacturing for aerospace application," Materials Research Express, **11**(2), 022001 (2024). https://doi.org/10.1088/2053-1591/ad21ad

[4] Nyamekye, P., Golroudbary, S. R., Piili, H., Kraslawski, A., & Luukka, P. "Impact of additive manufacturing on titanium supply chain: Case of titanium alloys in automotive and aerospace industries," Advances in Industrial and Manufacturing Engineering, **6**(C), 100112 (2023). https://doi.org/10.1016/j.aime.2023.100112

[5] Zhang, A., Li, Y., Xu, Q., Zhang, B., Qu, P., & Chen, W. "Application Status and Prospect of Titanium Alloys for Pressure-Resistant Structure of Deep-Sea Manned Equipment," Ship & Boat, **35**(06), 81 (2024). https://doi.org/10.19423/j.cnki.31-1561/u.2024.06.007

[6] Iskandarov, S. C., Khudaykulov, I. K., Turdaliev, T. K., Berdiyev, U. F., Tulaganov, S. A., & Kakhramonov, B. R. "Effect of TiO_2 Layer Thickness on Electrode Degradation in Redox Flow Batteries," East European Journal of Physics, (4), 601-606 (2025). https://doi.org/10.26565/2312-4334-2025-4-63

[7] Wang, L., Zhao, X., Wang, X., Shang, S., Xiu, Z., Xi, Y., *et al.*, "Current Status Review of Corrosion Resistance Applications of Titanium Alloys in the Petroleum Industry," Coatings, **14**(8), 941 (2024). https://doi.org/10.3390/coatings14080941

[8] Kumawat, S., Deshmukh, S.R., & Ghorpade, R.R. "Fabrication of Ti-6Al-4v cellular lattice structure using selective laser melting for orthopedic use: a review," Materials Today: Proceedings, **113**, 166-172 (2024). https://doi.org/10.1016/j.matpr.2023.08.053
[9] Yim, S., Minowa, K., Yamanaka, K., & Chiba, A. "Influence of particle size distribution on the powder bed quality in the powder bed fusion additive manufacturing process," Journal of Materials Research and Technology, (2025). https://doi.org/10.1016/j.jmrt.2025.06.136
[10] X.X. Yao, and Z. Zhang, "Laser-particle interaction-based heat source model of laser powder bed fusion additive manufacturing," Opt. Laser Technol. **155**, 108402 (2022). https:// doi. org/ 10. 1016/j. optla stec. 2022. 108402
[11] Xue, M., Chen, X., Ji, X., Xie, X., Chao, Q., & Fan, G. "Effect of particle size distribution on the printing quality and tensile properties of Ti-6Al-4V alloy produced by LPBF process," Metals, **13**(3), 604 (2023). https://doi.org/10.3390/met13030604
[12] Soltani-Tehrani, A., Yasin, M. S., Shao, S., Haghshenas, M., & Shamsaei, N. Effects of powder particle size on fatigue performance of laser powder-bed fused Ti-6Al-4V. Procedia Structural Integrity, **38**, 84-93 (2022). https://doi.org/10.1016/j.prostr.2022.03.010
[13] Çuvalcı, O., Varol, T., Akçay, S. B., Güler, O., & Çanakçı, A. "Effect of ball mill time and wet pre-milling on the fabrication of Ti powders by recycling Ti machining chips by planetary milling," Powder Technology, **426**, 118637 (2023). https://doi.org/10.1016/j.powtec.2023.118637
[14] Mendez-Lozano, N., Apátiga-Castro, M., Soto, K. M., Manzano-Ramírez, A., Zamora-Antuñano, M., & Gonzalez-Gutierrez, C. "Effect of temperature on crystallite size of hydroxyapatite powders obtained by wet precipitation process," Journal of Saudi Chemical Society, **26**(4), 101513 (2022). https://doi.org/10.1016/j.jscs.2022.101513
[15] Wu, J., Xia, M., Wang, J., Zhao, B., & Ge, C. "Effect of electrode induction melting gas atomization on powder quality: satellite formation mechanism and pressure," Materials, **16**(6), 2499 (2023). https://doi.org/10.3390/ma16062499
[16] Sojoodi, M., Behvar, A., Bajaj, H., Mohajerani, S., Vanaei, S., Taheri Andani, N., *et al*., "Integration of Circular Economy into Metal Additive Manufacturing: A Review of Ultrasonic Plasma Atomization for Producing Virgin and Recycled NiTi Powder," Shape Memory and Superelasticity, 1-41 (2025). https://doi.org/10.1007/s40830-025-00589-y
[17] Muthuswamy, P. "Influence of powder characteristics on properties of parts manufactured by metal additive manufacturing," Lasers in Manufacturing and Materials Processing, **9**(3), 312-337 (2022). https://doi.org/10.1007/s40516-022-00177-3
[18] Tammas-Williams, S., Withers, P. J., Todd, I., & Prangnell, P. B. "Porosity regrowth during heat treatment of hot isostatically pressed additively manufactured titanium components," Scripta Materialia, **122**, 72-76 (2016). https://doi.org/10.1016/j.scriptamat.2016.05.002
[19] Ludwig, I., & Kluge, M. "Investigation of an Increased Particle Size Distribution of Ti-6Al-4V Powders Used for Laser-Based Powder Bed Fusion of Metals," Materials, **17**(12), 2942 (2024). https://doi.org/10.3390/ma17122942
[20] Lanzutti, A., & Marin, E. "The challenges and advances in recycling/re-using powder for metal 3D printing: A comprehensive review," Metals, **14**(8), 886 (2024). https://doi.org/10.3390/met14080886
[21] Islam, S. F., Hawkins, S. M., Meyer, J. L., & Sharman, A. R. "Evaluation of different particle size distribution and morphology characterization techniques," Additive Manufacturing Letters, **3**, 100077 (2022). https://doi.org/10.1016/j.addlet.2022.100077
[22] Zhang, S., Guo, K., Qing, Y., & Liu, C. "Research progress on the preparation technology of spherical alloy powders for laser additive manufacturing," Materials, **18**(14), 3385 (2025). https://doi.org/10.3390/ma18143385
[23] Lewis, G. "Aspects of the powder in metal additive manufacturing: a review," World Journal of Engineering and Technology, **10**(2), 363-409 (2022). https://doi.org/10.4236/wjet.2022.102022
[24] Dwivedi, A. P., & Choudhury, S. K. "A Brief Study of the Particulate Matter Emissions During the EDM Process," in: *Green Buildings and Sustainable Engineering*, Springer, 2019. https://doi.org/10.1007/978-981-13-1202-1_39
[25] Wang, J., Sánchez, J. A., Wang, Z., Izquierdo, B., & Ayesta, I. "Observations on debris composition and size distribution in WEDM," Procedia CIRP, **95**, 331-336 (2020). https://doi.org/10.1016/j.procir.2020.02.323
[26] Oßwald, K., Woidasky, J., Hoffmann, A. M., & Moser, M. "Suitability of electrical discharge machining debris particles for usage as a powder for selective laser melting: an explorative study," Progress in Additive Manufacturing, **4**(4), 443-449 (2019). https://doi.org/10.1007/s40964-019-00080-y
[27] Rahmati, A., Abdullah, A., & Esmailnia, K. "Metal nanopowder production by cryogenic mechanical collision and pulsed electric discharge methods," (2021). arXiv preprint arXiv:2112.03055.
[28] Singh, A. K., Mahajan, R., Tiwari, A., Kumar, D., & Ghadai, R. K. "Effect of dielectric on electrical discharge machining: a review," in: *IOP Conference Series: Materials Science and Engineering*, **377**(1), 012184 (2018). https://doi.org/10.1088/1757-899X/377/1/012184
[29] Murti, V. S. R., & Philip, P. K. "An analysis of the debris in ultrasonic-assisted electrical discharge machining," Wear, **117**(2), 241-250 (1987). https://doi.org/10.1016/0043-1648(87)90258-4
[30] Khanra, A. K., Pathak, L. C., & Godkhindi, M. M. "Microanalysis of debris formed during electrical discharge machining (EDM)," Journal of Materials Science, **42**(3), 872-877 (2007). https://doi.org/10.1007/s10853-006-0020-0
[31] Painuly, M., Singh, R. P., & Trehan, R. "Electrochemical machining and allied processes: a comprehensive review," Journal of Solid State Electrochemistry, **27**(12), 3189-3256 (2023). https://doi.org/10.1007/s10008-023-05610-x
[32] Zhang, S., Zhou, J., Hu, G., Wang, L., & Xu, Y. "Process characteristics of electrochemical discharge machining and hybrid methods: a review," The International Journal of Advanced Manufacturing Technology, **129**(5), 1933-1963 (2023). https://doi.org/10.1007/s00170-023-12452-4
[33] Ben Mhahe, F., Zhang, Y., Chen, C., & Umoren, W. I. "Investigation of the influence of different types of electrolytes on the performance of the Electrochemical Discharge Machining process during micromachining of molybdenum," International Journal of Electrochemical Science, **19**(7), (2024). https://doi.org/10.1016/j.ijoes.2024.100647
[34] Rao, P. S., Sharma, V., Kumar, H., & Sushma, S. P. "Electro-Chemical Machining of Titanium Alloys and Various Composites for Efficient Machining Process: A Critical Review," Fabrication Techniques and Machining Methods of Advanced Composite Materials, 68-81 (2024).
[35] Zhang, L., Kong, L., Lei, W., & Li, Q. "Review of electrochemical discharge machining technology for insulating hard and brittle materials," Journal of the Brazilian Society of Mechanical Sciences and Engineering, **46**(3), 143 (2024). https://doi.org/10.1007/s40430-024-04739-8

[36] Singh, J., Kant, R., Nimesh, A., Katiyar, N., & Bhattacharya, S. "Evaluating electrochemical micromachining capabilities for industrial applications: A review," Materials and Manufacturing Processes, **39**(1), 1-42 (2024). https://doi.org/10.1080/10426914.2023.2219304
[37] Upadhyay, R. K. "Challenges and control strategies for disrupting passive oxide layer formation in electrochemical machining," Journal of Electrochemical Science and Engineering, **15**(5), (2025). http://dx.doi.org/10.5599/jese.2796
[38] Prakash, A., Kumar, A., & Ballav, R. "Process capability of electrochemical discharge machining: a review," Proceedings of the Institution of Mechanical Engineers, Part L: Journal of Materials: Design and Applications, **238**(2), 282-300 (2024). https://doi.org/10.1177/14644207231218386

ВПЛИВ КОНЦЕНТРАЦІЇ ЕЛЕКТРОЛІТУ ТА ЧАСТОТИ РОЗРЯДУ НА РОЗПОДІЛ РОЗМІРІВ ЧАСТИНОК ПОРОШКУ Ti-6Al-4V, ОТРИМАНОГО МЕТОДОМ ECDM

Б.А. Гоїпов, А.А. Зарiпов, У.Ф. Бердієв, Ш.Ч. Іскандаров, Т.К. Турдалієв, С.А. Тулаганов
Інститут іонно-плазмових та лазерних технологій імені У.А. Аріфова Академії наук Республіки Узбекистан,
100125, вул. Дурмон йулі, 33, Ташкент, Узбекистан

Метою цього дослідження є вивчення розподілу мікрочастинок порошку сплаву Ti-6Al-4V, що використовуються в 3D-друку, за різних частот розряду та концентрацій електроліту NaCl. У цій роботі проаналізовано процес отримання монодисперсних порошків зі сплаву Ti-6Al-4V за допомогою методу ECDM. Результати показали, що оптимальна концентрація електроліту NaCl становить 30 г/л, що забезпечує стабільне формування плазмових каналів і вузький розподіл розмірів частинок. Регресійний аналіз і низькі значення стандартної похибки (0,00386–0,00834) підтверджують високу керованість процесу. Також досліджувався вплив частоти на розмір частинок: при частоті 3,2 кГц було зафіксовано мінімальний середній розмір частинок — 16,598 мкм, тоді як збільшення частоти до 32 кГц призвело до зростання розміру частинок до 28,063 мкм через теплове накопичення. Результати показують, що як на частотах 3,2 кГц, так і 32 кГц від 58,24% до 68,89% вироблених порошків потрапляють у діапазон 15–55 мкм, необхідний для технології PBF-LB/M. Ці результати демонструють придатність отриманих порошків для технологій адитивного виробництва.

Ключові слова: *порошок Ti-6Al-4V; ECDM; адитивне виробництво; електроліт NaCl; концентрація електроліту; розподіл розмірів частинок; частота; регресійний аналіз*